Supporting Information for

Purcell enhancement of erbium ions in TiO_2 on silicon nanocavities

Alan M. Dibos,[*,†,‡] Michael T. Solomon,[¶,§,‡] Sean E. Sullivan,[§,‡] Manish K. Singh,[¶,§] Kathryn E. Sautter,[§,¶] Connor P. Horn,[¶,§] Gregory D. Grant,[¶,§] Yulin Lin,[†] Jianguo Wen,[†] F. Joseph Heremans,[§,‡,¶] Supratik Guha,[¶,¶,§] and David D. Awschalom[¶,§,‡]

†*Nanoscience and Technology Division, Argonne National Laboratory, Lemont, IL 60439*

‡*Center for Molecular Engineering, Argonne National Laboratory, Lemont, IL 60439*

¶*Pritzker School of Molecular Engineering, University of Chicago, Chicago, IL 60637*

§*Materials Science Division, Argonne National Laboratory, Lemont, IL 60439*

E-mail: adibos@anl.gov

1 Device simulations

Our 1D photonic crystal cavities are designed using 3D FDTD simulations (Lumerical) that employ electric dipole sources located close to the center of the cavity defect. The 14-hole cavity defect is created with a parabolic taper of the lattice constant[1] from 355 nm in the mirrors to 320 nm in the center of the cavity. All elliptical holes in a given waveguide are nominally identical with major and minor diameters of 397.5 nm and 195.0 nm, respectively. An autoconformal mesh is used for these simulations except for the TiO_2 layer which has an override mesh of 15 nm × 15 nm × 5 nm, to better resolve the field intensity in the thin layer of interest. The mode volume of the cavity is computed to be 0.038 μm^3, and calculated using:

$$V_{\text{mode}} = \frac{\int \mathrm{d}V\, \epsilon(\vec{r})|E(\vec{r})|^2}{\max(\epsilon(\vec{r})|E(\vec{r})|^2)}. \tag{1}$$

As discussed in the main text, our device geometry relies on the evanescent field in the Si waveguide coupling to ions in the nearby TiO_2 layer. Given the doping profile within the TiO_2 film, as shown in Figure 1a of the main text, an ideally positioned and aligned dipole within the doped layer will be TE-oriented (in the plane of the TiO_2 film and perpendicular to the waveguide direction) and in the center of the 14-hole cavity defect. If we assume that this dipole is positioned 10 nm above the Si/TiO_2 interface, which is near the center of the Er-doped region, it will be subject to approximately 37% of the maximum field intensity within the Si waveguide (Figure S1). For visual clarity, the magnitudes of the normalized intensities plotted in both Figure 1c in the main text and Figure S1 are relative to the maximum intensity in that particular plane, but the maximum intensity in Figure 1c is reduced by the evanescent coupling factor to 37% as shown in Figure S1. Based upon the dipole power output calculation within Lumerical, we estimate that this ideally placed dipole has a maximum Purcell factor near 1400, and the simulated Q for this cavity resonance (λ = 1536.40 nm at T=300 K) is 1.72×10^5. The cavity resonance will typically blueshift by 12 nm when cooled to T=3.1 K due to a change in the refractive indices; therefore, in order

to be resonant with the TiO_2 rutile transition at 1520.56 nm, devices are typically designed to be have a room temperature resonance near 1528 nm to account for this, whereby they can be subsequently gas condensation tuned across the rutile transition.

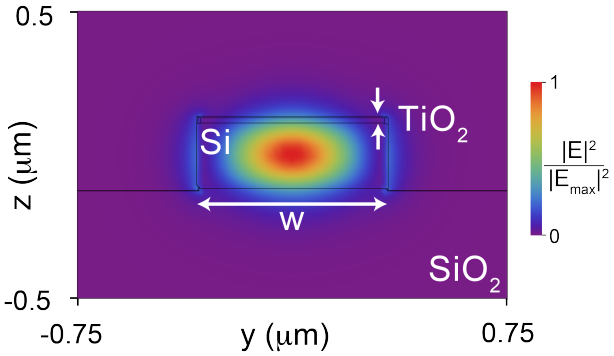

Figure S1: Cross-section of the electric field intensity in the waveguide through the center of the cavity. FDTD device simulation showing the moderate evanescent field intensity in the TiO_2 film relative to the Si waveguide. The width of the waveguide (w) is 671 nm, the thickness of the Si device layer is 220 nm, and the thickness of the TiO_2 is 22 nm.

2 Film growth, device fabrication, and electron microscopy

TiO_2 thin films are grown on diced pieces from 8" commercial SOI wafers (SOITEC). The Si device layer is lightly boron-doped with a resistivity of 10 Ω·cm. The TiO_2 thin film growth conditions and methods are outlined in Singh et al.[2] For this particular film the metallic Er source temperature is at 900° C, with an expected doping density of 35 ppm of Er^{3+}, to be later confirmed with secondary ion mass spectrometry. Following thin film growth, all device fabrication is performed in the Center for Nanoscale Materials cleanroom at Argonne National Laboratory. Device patterning is performed using electron beam lithography (JEOL 8100). The etch mask is a combination of electron-beam resist (ZEP 520A) and a plasma enhanced chemical vapor deposition (PECVD, Oxford PlasmaLab 100) SiO_2 hard-mask. Fluorine-based etching is used for mask transfer to the SiO_2, chlorine-based etching is used to etch through the TiO_2 layers, and HBr/O_2 is used to etch through the Si device layer. All etching is performed in an Oxford PlasmaLab 100 inductively coupled plasma (ICP) reactive ion etcher (RIE). Waveguide cleaving along alignment marks is performed

under an optical microscope (LatticeAx 420, LatticeGear). A full device fabrication flow is provided in Figure S2. The overall cavity reproducibility is very good. Within our large array of devices there are clusters of nominally identically designed cavities with the same hole size (the hole size is swept to account for run-to-run variations in the Si etch rate). Experimentally the cavity Qs at room temperature are within about 10% of each other and each resonance is typically within ∼1 nm of the other devices within the cluster. For TEM cross-section analysis, the opposite side of the cleaved chip shown in Figure 1d-e of the main text was mechanically ground to a thickness of 20 μm, followed by Ar ion milling to electron transparency. High-resolution TEM was performed at 200 kV using the Argonne chromatic aberration-corrected TEM (ACAT) also at the Center for Nanoscale Materials.

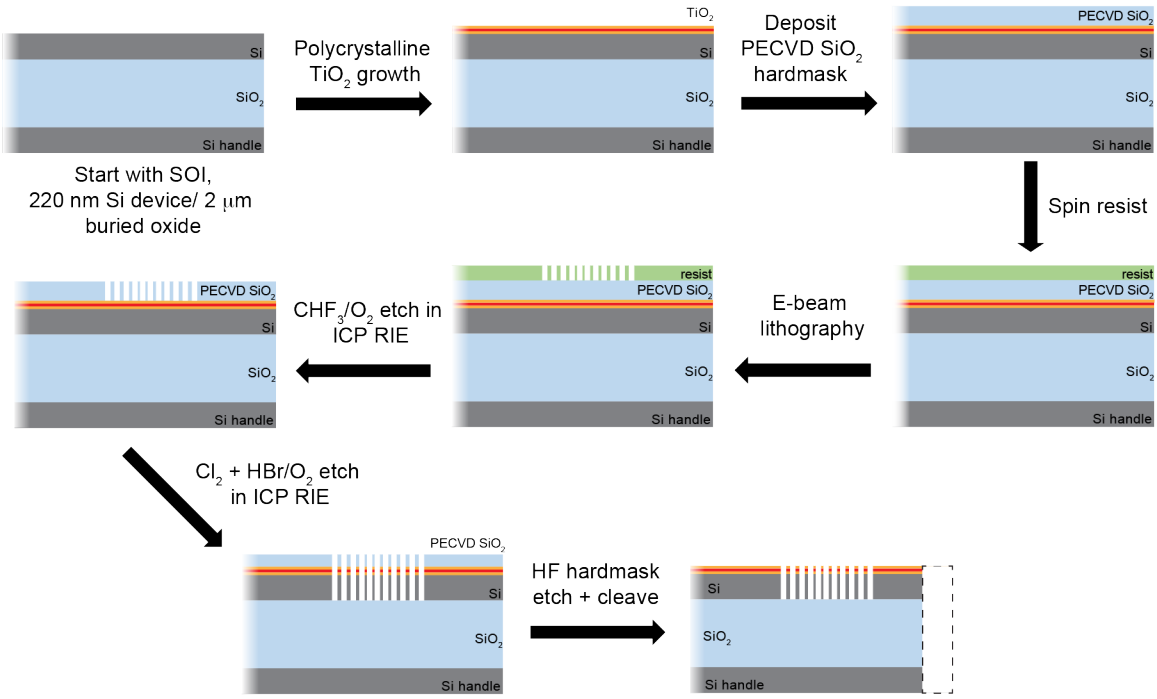

Figure S2: Fabrication flow. The fabrication flow used to generate 1D photonic crystal cavities from TiO_2 grown atop silicon-on-insulator (SOI) wafers. Note that the various layer thicknesses are not to scale.

3 Optical Characterization

Measurements are performed in a Montana Instruments S100 closed-cycle cryostat. The AR coated SMF-28 lensed fiber (TSMJ-X-1550-9/125-0.25-18-2.5-14-3-AR, OZ Optics) is mounted on an Attocube nanopositioner with 5 mm of x-y-z travel. The base temperature of the cold finger directly underneath the sample is measured to be 3.1 K. Resonant experiments are performed with a tunable telecom laser (CTL 1550, Toptica). The wavemeter used for wavelength measurement is a High Finesse WS8-10 with SLR-1532 calibration laser. The one-way coupling efficiency is estimated by measuring the ratio of the reflected laser power from a cavity device slightly off resonance to the laser power into the lensed fiber, and then taking the square root of this ratio. Our efficiency estimate of 15% encompasses all losses from the lensed fiber vacuum feedthrough to the device: including fiber bend losses, scattering along the inverse taper on the waveguide, and the fiber-waveguide coupling itself. However, due to the limitation that the waveguide be sufficiently wide to enable guiding and not lose light into the buried oxide layer, the mode mismatch between the waveguide and optical spot (~ 2.5 μm) of the lensed fiber is currently the dominant source of loss.

Pulses used for resonant laser pumping are generated with fiber acousto-optic modulators, AOMs (FiberQ, Gooch and Housego). The collective on/off ratio of these three modulators is greater than 150 dB. The typical pulses for waveguide-only devices are 0.1-1 ms long (CW laser power of 0.3-3 μW at the device) with collection times of 10-40 ms. Typical pulses for cavity-coupled ions are 1-10 μs long (CW laser power of $\sim$ 50 nW at the device) with collection times of 1-4 ms. The phase electro-optic modulator (MPZ-LN-10, iXblue) is driven with a vector signal generator (SG396, SRS) for sideband generation at a specified detuning from the laser carrier frequency. Single photon detection was performed with a SNSPD from Quantum Opus inside a second cryostat, which is designed for operation near 1550 nm with a dark/background count rate of 50 Hz and external quantum efficiency of 83%. In the collection path, an additional fiber AOM (MT80-IIR30-Fio-PM0.5-J1-A-Ic2, AA Opto

Electronic) is used to protect the SNSPD from direct laser exposure to mitigate transients in the detector signal. Single photon counting is performed using a dedicated time tagger (quTAG, qutools). Two voltage controlled fiber-coupled attenuators (V1550PA, Thorlabs) are used in series to control the incident laser power for resonant PLE experiments as well as in situ resonant laser cavity tuning. It is important to note that the fiber circulator is particularly useful—instead of a 99:1 fiber beam splitter, for example—because it allows for sufficiently high input powers at the device ($\sim$ 10 μW) after accounting for modulator and fiber-to-device losses. This enables resonant laser tuning of the cavity (via 2-photon absorption in Si) without an additional amplifier. This process generally works for the entire gas condensation tuning range of these devices of approximately 10 nm. Off-resonant PL measurements were performed by inserting a 1480 nm diode pump laser (QFBGLD-1480-300, QPhotonics) via a 1480/1550 nm fiber wavelength division multiplexer (WD1450A, Thorlabs). Erbium PL was detected after long-pass filtering (FELH1500, Thorlabs) using a spectrometer (IsoPlane SCT320, Princeton Instruments) equipped with a PyLoN-IR liquid-nitrogen cooled InGaAs camera. The spectrometer has a 600 groove/mm grating, and the resolution of $\sim$ 0.1 nm was confirmed by measuring a narrow line width laser.

In Figure S3 we re-plot the bare waveguide and cavity-coupled linear-log decay curves from Figure 3b of the main text on a log-linear scale, and it is clear that the ensemble decay curves are not single exponential in nature. The dark counts are subtracted off to account for the vastly greater number of pulse loops for the bare waveguide experiment. The bare waveguide decay curves are normalized and fit with a single stretched exponential of the form $I(t) = B\exp(-t/\tau_{slow})^{F_{slow}} + C$ to account for the variation in coupling for ions in the ensemble[3] (dashed gray line, corresponding to parameters: B=0.978(0.003), τ_{slow}=4660(20) μs, F_{slow}=0.745(0.003), and C=0.023(0.003)). For the cavity coupled ions, we use the sum of a fast decaying stretched exponential and a slow single exponential to account for contributions of the fast decaying cavity-coupled ions and the slowly decaying uncoupled ions along the waveguide. The shorter decay time of the cavity coupled ions mitigates

the need for a second stretched exponential to capture the bare waveguide ion dynamics. This combined fit is of the form: $I(t) = A\exp(-t/\tau_{fast})^{F_{fast}} + B\exp(-t/\tau_{slow}) + C$ (dashed black line, corresponding to parameters: A=0.926(0.013), τ_{fast}=23(1) μs, F_{fast}=0.60(0.01), B=0.058(0.003), τ_{slow}=4340(620) μs, and C=0.016(0.003)). The bare waveguide decay time is the starting point for the fit of the slower components in the two exponential fit, as can be seen qualitatively in the approximate slopes of the slow components in Figure S3. The raw decay curves are fit with a non-linear model fit in Mathematica, weighing each point by its shot noise and taking the standard error with the uncertainty at the 95% confidence level. It is important to note that for these measurements, τ_{fast} physically represents the fastest decay time within the cavity-coupled ensemble, and **the specific fit for τ_{fast} is very robust regardless of the other parameters** (A, B, F_{fast}, τ_{slow}, and C).

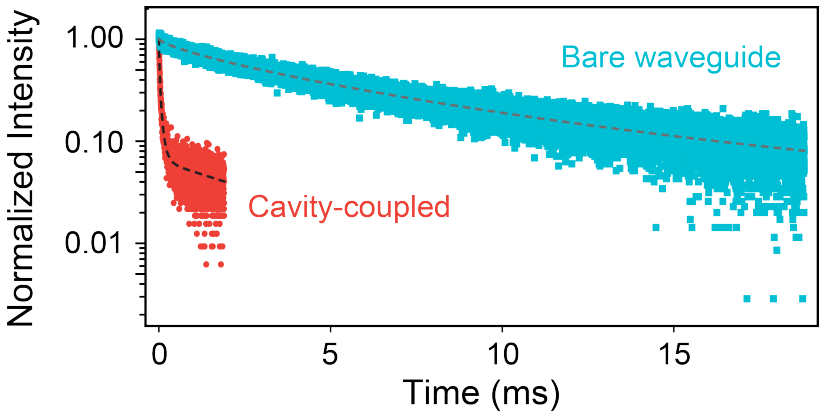

Figure S3: Stretched exponential fitting of decay curves. PLE decay curves identical to that shown in Figure 3b of the main text, except re-plotted on log-linear scale to emphasize the stretched exponential nature of the decay for both the bare waveguide and cavity coupled devices. Dashed lines are fits as discussed above.

At the present time it is challenging to accurately estimate the number of ions that can couple to the cavity due to the spatial, crystalline phase, and dipolar inhomogeneities of the Er^{3+} ions in the TiO_2. However, if we merely start with basic device parameters such as: the Er doping density (35 ppm), thickness of the doped layer (7.5 nm), waveguide width (671 nm), averaged density of anatase and rutile phases of TiO_2 (4 g/cm^3), and a coarse approximation of the cavity length (3 μm), we estimate that there are roughly 1.4×10^4 erbium ions in the cavity. We do not know the actual percentage of Er ions

residing in rutile, anatase, or interstitial sites; however, we can roughly estimate—based upon the photoluminescence (PL) data shown in Figure 2b of the main text—that between 10-50% of ions are in the rutile phase. This large uncertainty is because the off-resonant PL is a CW brightness measurement without regard to the optical lifetime of Er in each site. We then estimate that using our resonant laser excitation, we pump approximately 300 MHz (homogeneous line width estimate) of the the roughly 50 GHz ensemble inhomogeneous line width (0.6% of those ions) with our narrowband laser. Overall, we estimate that there are between 9 and 45 Er ions in rutile that can couple to the cavity.

This total ion number is in reasonable agreement with the number of photons detected in the resonant PLE cavity data corresponding to Figure 3b of the main text. We can first estimate the total number of photons detected after a single pulse in the short collection window (230 μs) corresponding to a Purcell factor near 20. We can then interpolate the number of PLE photons generated in the cavity after accounting for various loss channels in the experimental collection pathway: the cavity mode collection efficiency (28%), waveguide-to-fiber efficiency (15%), fiber network losses including collection channel AOM (46%), and SNSPD quantum efficiency (83%). If we assume that, given the relatively short pump pulse length, each photon can only correspond to one ion excited, we estimate that using our relatively low laser pump power, roughly 7 ions are excited after a single 10 μs laser pulse resonant with the rutile transition. This can be compared to the total number of photons injected into the cavity during the PLE experiment, which we estimate to be roughly 1×10^4 photons per pulse.

As discussed in the main text, there is a modest reduction in the cavity quality factor of $\sim 20\%$ as the cavity is tuned through the TiO_2 rutile transition near 1520.56 nm (Figure S4). The Q-factors were obtained from the FWHM of Lorentzian fits to reflection measurements taken periodically during the long cavity resonance tuning of the experiment (> 8 hours). The cavity line width when exactly resonant is 5.10(0.12) GHz, which is in excellent agreement with the overall line width of the ensemble decay rate versus cavity-laser detuning when

the laser is fixed at 1520.56 nm (5.06(0.17) GHz, as shown in Figure 3c of the main text). This agreement further corroborates that the decay rate enhancement demonstrated is due to the presence of the cavity. However, this particular trend of the Q-factor reduction and recovery was unique to this experimental run, and while physically accurate it is not a reproducible feature of tuning a cavity through this spectral range (e.g. parasitic absorption). At the present time, we do not understand the cause of this slow drift of the Q-factor over the course of the experiment and additional measurements on control samples are needed.

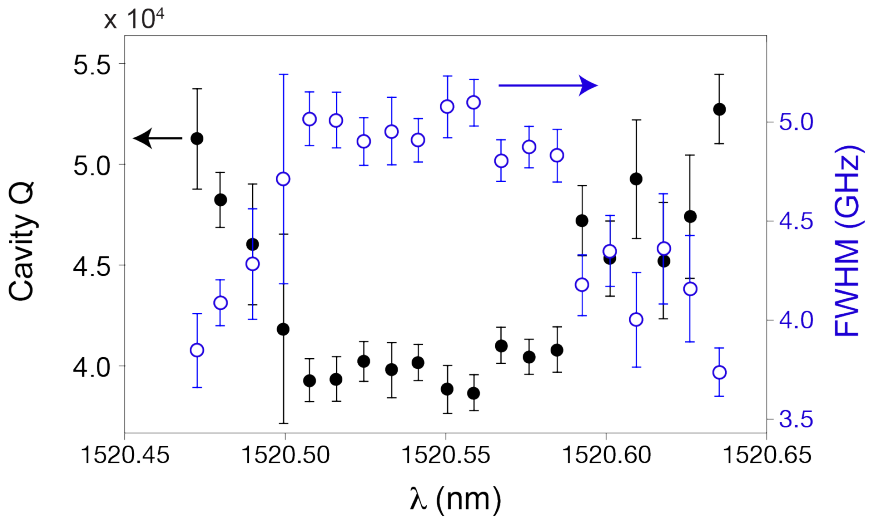

Figure S4: Reduction in cavity quality factor near Er transition in rutile TiO_2. A plot of the cavity quality factor (Q) at T = 3.1 K as measured by resonant laser reflection scan (left axis) as the cavity is systematically redshifted through the Er:rutile TiO_2 transition at 1520.56 nm. The associated cavity line width (FWHM in GHz, right axis) as the cavity is detuned is also shown.

References

(1) Dibos, A. M.; Raha, M.; Phenicie, C. M.; Thompson, J. D. Atomic Source of Single Photons in the Telecom Band. *Physical Review Letters* **2018**, *120*, 243601.

(2) Singh, M. K.; Wolfowicz, G.; Wen, J.; Sullivan, S. E.; Prakash, A.; Dibos, A. M.; Awschalom, D. D.; Heremans, F. J.; Guha, S. Development of a Scalable Quantum Memory Platform – Materials Science of Erbium-Doped TiO_2 Thin Films on Silicon. **2022**, 2202.05376v2. *arXiv (Condensed Matter, Materials Science)*; `http://arxiv.org/abs/2202.05376`, (accessed: April 10, 2022).

(3) Van de Walle, C. G. Stretched-exponential relaxation modeled without invoking statistical distributions. *Physical Review B - Condensed Matter and Materials Physics* **1996**, *53*, 11292–11295.